


Testing the validity of supersonic molecular beam modeling in the high-throughput range using an Even-Lavie valve

Simen K. Hellner ^{1,*}, Sabrina D. Eder ¹, Gianangelo Bracco ² and Bodil Holst ¹

¹*Institute of Physics and Technology, University of Bergen, 5007 Bergen, Norway*

²*CNR-IMEM, Department of Physics, University of Genova, Via Dodecaneso 33, 16146 Genova, Italy*

 (Received 10 July 2023; revised 4 February 2024; accepted 23 February 2024; published 19 March 2024)

Supersonic molecular beams are used in several scientific fields ranging from surface science to the spectroscopy of molecules, nanoparticles, and even viruses. It is therefore of interest to understand the fundamental properties of the expansion and resulting beam. Here, we present a study of the change in the most probable velocity with reservoir pressure, using a so-called Even-Lavie pulsed source with a 200- μm -diam nozzle. Experiments were carried out in the throughput range $p_0d = 400\text{--}2000$ mbar cm, where p_0 is the reservoir stagnation pressure and d is the nozzle diameter. Experiments were done on both neutral and metastable helium beams. A two-detector measurement setup was used to account for the valve opening delay. The measurements are modeled with theory which has hitherto only been applied to a p_0d regime up to 190 mbar cm, showing good agreement.

DOI: [10.1103/PhysRevA.109.032813](https://doi.org/10.1103/PhysRevA.109.032813)

I. INTRODUCTION

Supersonic helium beams are used for a wide range of applications. Uses for neutral, ground state helium beams include microscopy [1–3], surface science [4–8], and seeded beam experiments [9,10]. Metastable helium beams are used among others in spectroscopy and material characterization experiments [11–13], for lithography [14–17], for fundamental atom physics experiments on the lifetime of atomic states [18,19], for Bose-Einstein condensate generation, and for other fundamental studies related to beam properties [20,21].

Supersonic beams are made by an adiabatic expansion of the gas from a high-pressure reservoir through a nozzle with a diameter larger than the mean free path of the particles in the gas reservoir. This leads to a high-intensity beam with a velocity distribution which is significantly narrower than its effusive beam counterpart [22] (where the diameter of the nozzle is smaller than the mean free path). Supersonic molecular beam sources come in continuous or pulsed varieties. A pulsed beam enables an increase in intensity over the duration of the beam pulse compared to a continuous one for a given pumping system [23–25]. In the experiments presented here, we use a so-called Even-Lavie valve [26,27] pulsed source. The Even-Lavie valve is commercially available and is used to generate molecular beams for a wide range of applications including the previously mentioned fields of study (see also Refs. [28–31]). The behavior and characteristics of supersonic helium beam expansions have been investigated in a range of experiments and theoretical works [32–35]. A summary is included in a review of neutral helium microscopy by Palau *et al.* [36]. Of particular interest here is work related to

measurements and the prediction of the most probable velocity of the helium atoms in the beam. The effect of varying nozzle size and source stagnation pressure has so far to the best of our knowledge only been measured for the p_0d (source stagnation pressure \times nozzle diameter) regime up to 190 mbar cm [37]. Here, we present measurements of the most probable velocity of the helium beam from the Even-Lavie valve up to 2000 mbar cm and compare them to theoretical modeling first presented by Reisinger *et al.* [38]. The theory has been used in several other investigations, for example, in explorations of the center-line beam intensity [35].

II. EXPERIMENTAL SETUP

Experiments were performed with a room-temperature Even-Lavie pulsed valve source purchased from the company LAMID Multidisciplinary Instruments Development. The source has a 200- μm -diam trumpet-shaped expansion nozzle [33]. Experiments were done using ground state and metastable helium beams. The experiments performed with metastable helium atoms use the dielectric barrier discharge unit (DBD) mounted in the front of the nozzle [27]. The DBD unit is explained in greater detail by Luria *et al.* [34]. A three-dimensional (3D) diagram of the Even-Lavie pulsed valve with the DBD unit as well as a cross section of the DBD unit is shown in Fig. 1. For the experiments presented here, the original preionizer “electron brush” from the supplier was replaced by an ionizing filament supplied with 12 V and a heating current set above the level required for ignition. The filament is mounted in front of the nozzle opening. For the neutral helium measurements, the source was mounted on the molecular beam apparatus at the University of Bergen known familiarly as MAGIE [39]. For the metastable helium measurements, the source was mounted in another setup

*simen.hellner@uib.no

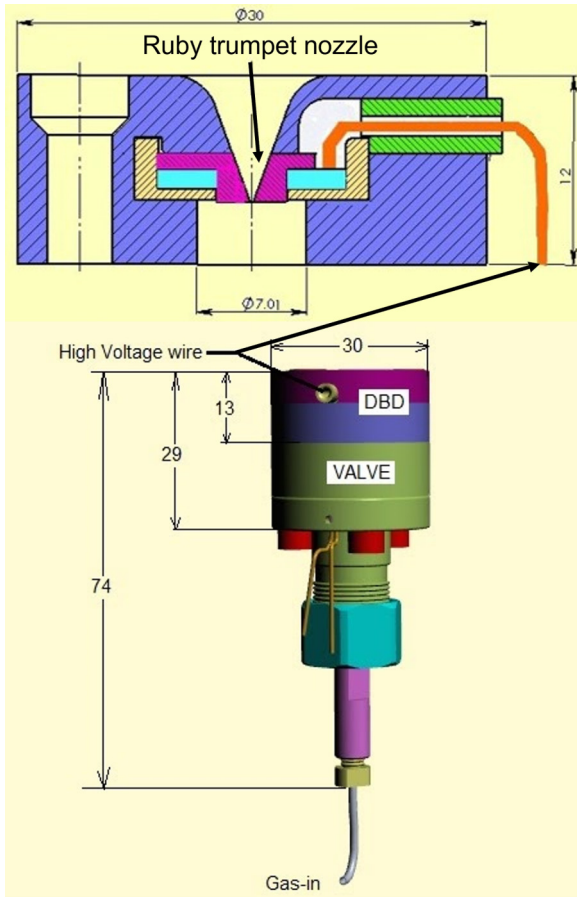


FIG. 1. Schematic cross section of the Even-Lavie pulsed valve (room-temperature model) and the dielectric barrier discharge (DBD) unit, responsible for exciting the helium atoms to a metastable state. Trumpet-shaped ruby expansion nozzle (200 μm diameter). The numbers show dimensions in mm. Figures from the manufacturer's website [27].

where the time of flight (TOF) could be measured at two different locations along the beamline. In both setups, the central part of the beam was selected by letting the beam pass through a 3-mm skimmer (Beam Dynamics, model 2), located 492 mm (neutral) and 374 mm (metastable) downstream from the nozzle opening. The MAGIE source chamber has dimensions $492 \times 600 \times 510 \text{ mm}^3$ ($V = 0.15 \text{ m}^3$) and is pumped by a 3200 l/s turbomolecular pump (Leybold MAG W 3200), backed by a $65 \text{ m}^3/\text{h}$ rotary vane pump (Leybold TRIVAC D65B) and two single roots blowers of $505 \text{ m}^3/\text{h}$ (Leybold RUVAC WS501) and $253 \text{ m}^3/\text{h}$ (Leybold RUVAC WS251). The second setup has a source chamber volume of 0.045 m^3 and a total of 3600 l/s pumping capacity from $3 \times$ Leybold MAG W, backed by a $55 \text{ m}^3/\text{h}$ multistage roots pump (Leybold ECODRY 65 Plus).

Figure 2(a) shows a diagram of the neutral helium detector setup. Figure 2(b) shows a diagram of the metastable helium setup. Please note here the use of two detectors along the beamline. This was used to be able to account for the initially unknown internal, pressure-dependent delay in the valve mechanism. For all experiments the source was left running for 1 h before measuring to ensure a stable operation

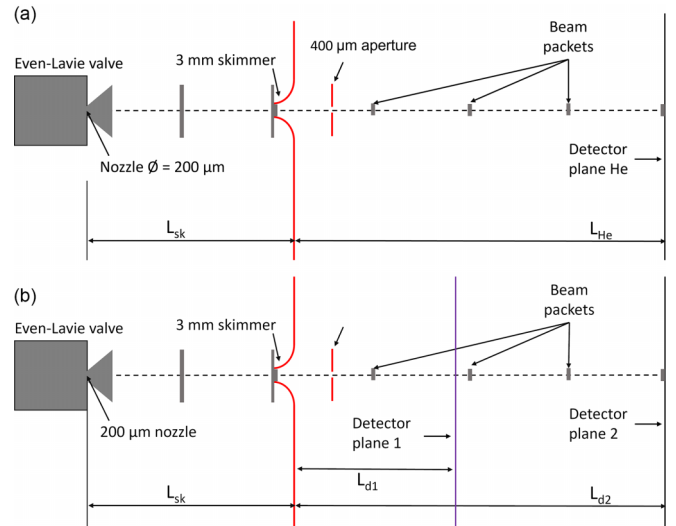


FIG. 2. (a) Schematic of the neutral helium beam setup. The distances L_{sk} (492 mm) and L_d (3240 mm) are the distances from the nozzle to the skimmer and detector, respectively. (b) Schematic of the metastable helium beam setup. Two detectors are used to account for the effects of internal delay in the valve. The distances L_{sk} (374 mm), L_{d_1} (604 mm), and L_{d_2} (1024 mm) are the distances from the nozzle to the skimmer and the two detectors, respectively.

temperature, because it had been observed from the beam performance that the nozzle initially heats up during operation. Unfortunately, it was not possible to measure the temperature of the nozzle directly in the current setup.

A. TOF experimental method 1: Neutral He

The neutral He time-of-flight (TOF) spectra were recorded using an ionization detector located 3240 mm from the source nozzle opening [2748 mm from the skimmer (L_{He})]. The distance from the source to the skimmer (L_{sk}) was 492 mm. The signal sent from the source controller to trigger the Even-Lavie valve was also used as the trigger ($t = 0$) for the TOF measurement. A 400- μm aperture was placed 960 mm downstream after the skimmer to avoid saturation in the detector. The background pressure never exceeded 1.2×10^{-4} mbar in the source chamber and 3×10^{-7} mbar in the rest of the instrument. Please note that all pressure measurements in the source chamber have been corrected for helium with the correction factor [40] $K = 5.9$. The source was running at a repetition rate of 100 Hz and TOF spectra were recorded for every 10 bars of source pressure (p_0) from 20 to 100 bars, in random order. The DBD unit was not operated during these measurements. An example of a TOF spectrum, recorded at $p_0 = 100$ bars, can be seen in Fig. 3 (top).

B. TOF experimental method 2: Metastable He* differential TOF

The second set of TOF spectra were recorded in a setup with two detectors [see Fig. 2(b)]. The detectors were located 604 and 1024 mm from the nozzle, respectively. The TOF spectra were recorded by collecting the metastable He* atoms

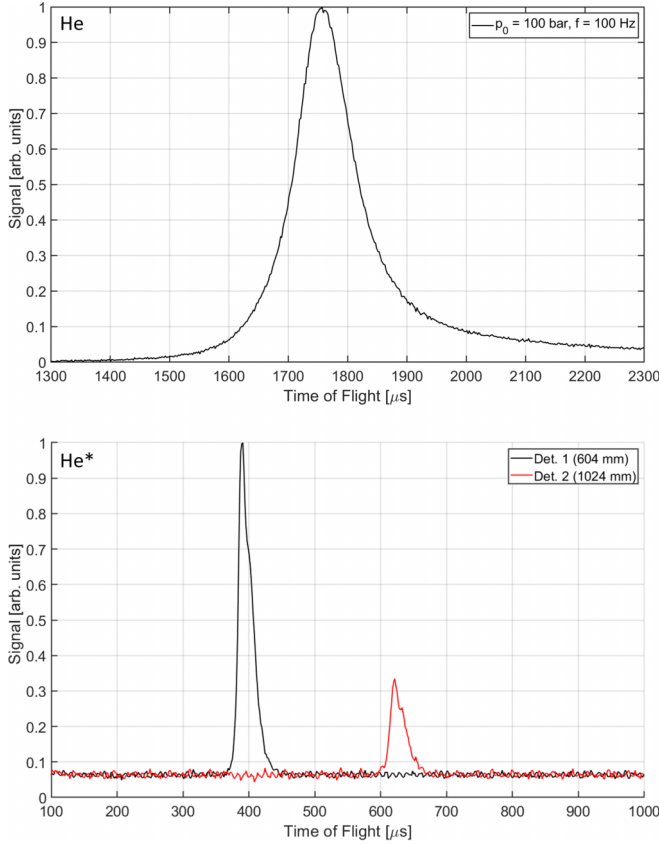


FIG. 3. Raw time-of-flight measurements of neutral helium (top) and metastable helium (bottom). The source pressure is 100 bars and the source repetition rate, $f = 100$ and 10 Hz, respectively. The neutral He detector is located 3240 mm from the source. Two detectors were used for the metastable helium measurements, located 604 and 1024 mm from the source nozzle, respectively.

on a 4-mm-diam stainless steel plate. When a metastable helium atom hits the detector plate, it decays leading to emission of an electron. Measuring the current on the plate thus gives a measure of the incident metastable helium signal [41]. Using the same trigger as for the neutral He TOF measurements, the measured current signal from the detector plate also provides a TOF spectrum. Using the peak values (i.e., the most probable TOF) obtained from the two detectors, the true, delay-independent, most probable velocity V was calculated by $V = (L_{d_2} - L_{d_1})/\Delta t$, where Δt is the difference in measured TOF between the two detectors and L_{d_1} and L_{d_2} are the flight distances [see Fig. 2(b)]. From these measurements, we also obtained values for the pressure-dependent valve delay of the source, as shown in Fig. 4. The measured signal from a single pulse is low compared to background noise, therefore the measurements were done by averaging over 8 pulses per recorded spectrum, an example of a measurement can be seen in Fig. 3 (bottom). The source was running with a repetition rate of 10 Hz and the measurements were again performed two times per set for source pressures 20–100 bars in 10-bar increments. A total of five sets of two measurement series were performed at different times, due to fluctuating valve delay as shown in Fig. 4. The chamber pressure was always below

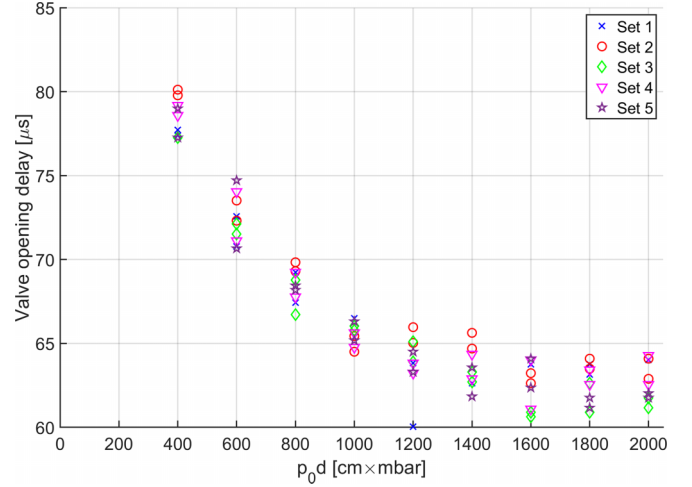


FIG. 4. The valve delay measured as a function of source pressure. The five measurement sets were taken at five different times.

10^{-5} mbar in the source chamber and 10^{-8} mbar in the rest of the instrument.

C. Theoretical model

The gas expansion is described by using a theoretical model based on the solution of the Boltzmann equation by means of the moment method [42], which has successfully been used in previous studies for lower throughputs as mentioned in the Introduction [37]. In this approach, since the expanding gas is not in equilibrium, two different temperatures are assumed for the motion parallel (T_{\parallel}) or perpendicular (T_{\perp}) to the streamlines with the expansion assumed spherically symmetric [43]. Therefore the real distribution is approximated by the anisotropic ellipsoidal Maxwell velocity distribution

$$f_{\text{aeM}}(\vec{v}) = n \left(\frac{m}{2\pi k_B T_{\parallel}} \right)^{\frac{1}{2}} \left(\frac{m}{2\pi k_B T_{\perp}} \right) \times \exp \left(-\frac{m}{2k_B T_{\parallel}} (v_{\parallel} - V)^2 - \frac{m}{2k_B T_{\perp}} v_{\perp}^2 \right)$$

where k_B is the Boltzmann constant, n is the number density, m the He mass, V is the most probable velocity of the expanding gas, and v_{\parallel} and v_{\perp} are the parallel and perpendicular components of the velocity \vec{v} , respectively.

The collisions, that determine the evolution of the parameters n , V , T_{\parallel} , and T_{\perp} in the expanding gas, are described by the collision integral

$$\Omega^{(2,1)}(T_{\text{eff}}) = \left(\frac{k_B T_{\text{eff}}}{\pi m} \right)^{\frac{1}{2}} \int_0^{\infty} Q^{(2)}(E) \gamma^5 \exp(-\gamma^2) d\gamma, \quad (1)$$

where T_{eff} is an effective average temperature varying between T_{\perp} and T_{\parallel} , E is the collision energy of two atoms in the center-of-mass system, $\gamma = \sqrt{\frac{E}{k_B T_{\text{eff}}}}$, and $Q^{(2)}(E)$ is the viscosity cross section.

The viscosity cross section for Bose-Einstein particles is expressed by

$$Q^{(2)}(E) = \frac{8\pi\hbar^2}{mE} \sum_{0,2,4,\dots} \frac{(l+1)(l+2)}{2l+3} \sin^2(\eta_{l+2} - \eta_l), \quad (2)$$

where η_l is the phase shift of the partial wave with orbital angular momentum l and the sum is evaluated on even values. For the calculation of phase shifts, the spherically symmetric He-He interaction was assumed to be a Lennard-Jones potential which has proven to provide good results for explaining the properties of He beams generated by a source at room temperature [37]. The Schrödinger equation for the radial wave function, apart the Lennard-Jones potential, contains the centrifugal potential which depends on angular momentum and this equation has been solved by a numerical integration based on the Runge-Kutta method for a collision energy E . At sufficiently large distance, the behavior of the wave function allows the estimation of the phase shifts for any orbital angular momentum l . An iterative procedure estimates phase shifts increasing the distance until the difference between phase shifts at two subsequent iterations is less than 0.005. Then Eq. (2) is evaluated taking into account more l terms until a new term increases the sum for less than 0.005. This procedure has been repeated for different collision energies E in order to generate a numerical approximation to $Q^{(2)}(E)$ for the interpolation scheme employed in the evaluation of the collision integral Eq. (1). Finally, a set of four equations to be solved is derived for the moments of the anisotropic distribution, i.e., gas density, most probable velocity, parallel and perpendicular temperatures, as was described in Ref. [43].

As a conclusive remark of this theoretical section, we observe that other studies on the supersonic beam expansion performed at low temperatures have shown the importance of including real gas properties even for helium [44,45]. In our case, where the source is operated around room temperature, this effect could be considered less relevant. Therefore the simple assumption of enthalpy independent on the source pressure, especially for helium which is considered an example of a perfect gas, may be taken for granted providing a constant terminal speed $V = \sqrt{\frac{5k_B T_0}{m}}$. On the contrary, the collected data have shown that V indeed depends on the source pressure, therefore the present calculations were carried out including the enthalpy based on the helium equation of state obtained by McCarty [46].

III. RESULTS AND ANALYSIS

Figure 3 shows examples of TOF spectra for the two experimental methods. From the neutral He TOF spectra, the most probable velocity V was calculated, from the TOF peak time t and the source-detector distance L as $V = L/t$. The most probable velocity of the metastable He* atoms was calculated by finding the peak time t of the TOF spectra from both detectors [Fig. 3 (bottom)] and using the distance between them to calculate the most probable velocity by $V = (L_{d_2} - L_{d_1})/\Delta t$. The five sets of metastable measurements (ten measurements

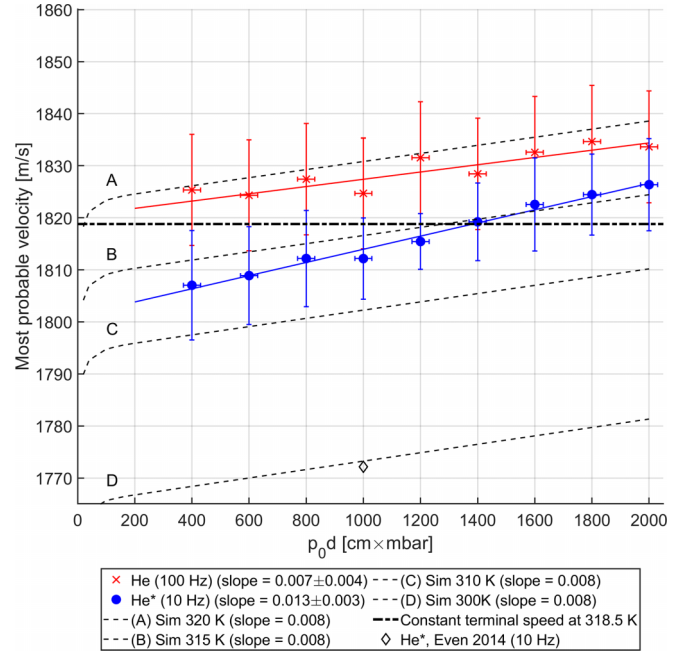


FIG. 5. The measured most probable velocity as a function of the source pressure and nozzle diameter for the two experimental setups, as well as the value measured by Even in 2014 [47]. The points in the figure represent the average measured values. Linear fits were made for the measurements and the slope was calculated for each. The error of the slopes represents the 95% confidence level interval. The measurements are compared to simulations using the model described in Sec. II C, for the temperatures 300, 310, 315, and 320 K. The predicted velocity for an ideal helium gas at 318.5 K is shown as a dashed-dotted line. Note also the good agreement with previous room-temperature measurements.

per $p_0 d$ in total) have been averaged and the error bars represent the standard deviation. The measurement error of the neutral He measurements was obtained from an estimation of the accuracy by which we can determine the peak positions and there is an additional error contribution of $2 \mu\text{s}$ in the time of flight, due to the bin size of $4 \mu\text{s}$ of the neutral He TOF measurement setup. The most probable velocity of the He and He* atoms as a function of $p_0 d$, where p_0 is the source pressure (or reservoir pressure) and d is the nozzle diameter, are shown in Fig. 5 together with theoretical predictions for temperatures 300, 310, 315, and 320 K, as described in Sec. II C. The measurements were fitted with a linear fit in accordance with the theoretical prediction. The slope of the fits is displayed in the legend of Fig. 5, together with the 95% confidence level interval for each fit. All measurements show an increase in the most probable velocity with increasing source pressure as predicted by theory. Considering the slopes of the fits, the agreement between theory and experiments is excellent for the neutral helium beams. This agreement allows us to estimate that the gas stagnation temperature is slightly less than 320 K, around 318.5 K. At this temperature the constant terminal speed value is 1818.8 m/s, which is also shown in Fig. 5 as a dashed-dotted line. Its trend clearly does not represent the measured points. For the metastable helium beams,

the slope is slightly higher than predicted by the theory. We suggest that this must be an effect caused by the excitation process. The difference between the most probable velocities of the neutral beams and the metastable beams is likely due to the different source repetition rates. The neutral helium measurements were performed with a source repetition rate of 100 Hz, whereas the metastable helium measurements were performed at a source repetition rate of 10 Hz. It is probable that this leads to an increase in nozzle temperature, increasing the velocity of the exiting gas.

We include also a published velocity measurement from Even *et al.* [47], obtained by determining the peak position of the TOF measurement in Fig. 10 in Ref. [47] and calculating the velocity from the flight distance also provided in the reference. This measurement is obtained with a pressure of 50 bars and a source repetition rate of 10 Hz [48]. It is stated in the paper that the measurement is carried out at 300 K, in good agreement with our theoretical prediction.

IV. CONCLUSION

We present measurements of the most probable velocity for a supersonic helium expansion close to room temperature in the throughput regime $p_0d = 400\text{--}2000$ mbar cm. The measurements have been compared to an existing theoretical model that is tested in this regime. Measurements are presented for neutral and metastable helium beams. For the neutral helium beams the increase in most probable velocity with p_0d is in excellent agreement with theory. For the metastable helium beams it appears that the increase is slightly bigger than predicted. We suggest that this is due to the excitation mechanism.

ACKNOWLEDGMENTS

This work was funded by the European Union's Horizon 2020 Research and Innovation Programme H2020-FETOPEN-2018-2019-2020-01 under Grant Agreement No. 863127 nanoLace.

-
- [1] S. D. Eder, A. Fahy, M. G. Barr, J. R. Manson, B. Holst, and P. C. Dastoor, Sub-resolution contrast in neutral helium microscopy through facet scattering for quantitative imaging of nanoscale topographies on macroscopic surfaces, *Nat. Commun.* **14**, 904(2023).
 - [2] A. S. Palau, G. Bracco, and B. Holst, Theoretical model of the helium pinhole microscope, *Phys. Rev. A* **94**, 063624 (2016).
 - [3] A. Salvador Palau, G. Bracco, and B. Holst, Theoretical model of the helium zone plate microscope, *Phys. Rev. A* **95**, 013611 (2017).
 - [4] G. Bracco and B. Holst, *Surface Science Techniques*, (Springer, Berlin, 2013), Vol. 51, Chap. 12, pp. 333–367
 - [5] G. Brusdeylins, R. B. Doak, and J. P. Toennies, High-resolution helium time-of-flight studies of Rayleigh surface-phonon dispersion curves of LiF, NaF, and KCl, *Phys. Rev. B* **27**, 3662 (1983).
 - [6] D. Farias and K.-H. Rieder, Atomic beam diffraction from solid surfaces, *Rep. Prog. Phys.* **61**, 1575 (1998).
 - [7] S. D. Eder, S. K. Hellner, S. Forti, J. M. Nordbotten, J. R. Manson, C. Coletti, and B. Holst, Temperature-dependent bending rigidity of *ab*-stacked bilayer graphene, *Phys. Rev. Lett.* **127**, 266102 (2021).
 - [8] M. Tømterud, S. D. Eder, C. Büchner, L. Wondraczek, I. Simonsen, W. Schirmacher, J. R. Manson, and B. Holst, Observation of the boson peak in a two-dimensional material, *Nat. Phys.* **19**, 1910 (2023).
 - [9] P. Gorry, C. Nowikow, and R. Grice, Reactive scattering of a helium seeded oxygen atom beam, *Chem. Phys. Lett.* **49**, 116 (1977).
 - [10] E. Kolodney and A. Amirav, Aerodynamical acceleration and rotational-vibrational temperatures in seeded supersonic molecular beams, *Chem. Phys.* **82**, 269 (1983).
 - [11] H. Morgner, The characterization of liquid and solid surfaces with metastable helium atoms, *Adv. At., Mol., Opt. Phys.* **42**, 387 (2000).
 - [12] S. Falcinelli, P. Candori, M. Bettoni, F. Pirani, and F. Vecchiocattivi, Penning ionization electron spectroscopy of hydrogen sulfide by metastable helium and neon atoms, *J. Phys. Chem. A* **118**, 6501 (2014).
 - [13] N. Bonini, G. P. Brivio, and M. I. Trioni, Theory of metastable deexcitation spectroscopy on simple metals, *Phys. Rev. B* **68**, 035408 (2003).
 - [14] T. Nesse, J.-P. Banon, B. Holst, and I. Simonsen, Optimal design of grid-based binary holograms for matter-wave lithography, *Phys. Rev. Appl.* **8**, 024011 (2017).
 - [15] J. Fiedler and B. Holst, An atom passing through a hole in a dielectric membrane: impact of dispersion forces on mask-based matter-wave lithography, *J. Phys. B: At., Mol. Opt. Phys.* **55**, 025401 (2022).
 - [16] C. S. Allred, J. Reeves, C. Corder, and H. Metcalf, Atom lithography with metastable helium, *J. Appl. Phys.* **107**, 033116 (2010).
 - [17] W. Lu, K. G. H. Baldwin, M. D. Hoogerland, S. J. Buckman, T. J. Senden, T. E. Sheridan, and R. W. Boswell, Sharp edged silicon structures generated using atom lithography with metastable helium atoms, *J. Vac. Sci. Technol. B* **16**, 3846 (1998).
 - [18] S. S. Hodgman, R. G. Dall, L. J. Byron, K. G. H. Baldwin, S. J. Buckman, and A. G. Truscott, Metastable helium: A new determination of the longest atomic excited-state lifetime, *Phys. Rev. Lett.* **103**, 053002 (2009).
 - [19] R. S. Van Dyck, C. E. Johnson, and H. A. Shugart, Radiative lifetime of the 2^1s_0 metastable state of helium, *Phys. Rev. A* **4**, 1327 (1971).
 - [20] A. S. Tychkov, T. Jeltens, J. M. McNamara, P. J. J. Tol, N. Herschbach, W. Hogervorst, and W. Vassen, Metastable helium Bose-Einstein condensate with a large number of atoms, *Phys. Rev. A* **73**, 031603(R) (2006).
 - [21] K. Baldwin, Metastable helium: Atom optics with nanogrenades, *Contemp. Phys.* **46**, 105 (2005).

- [22] G. Scoles, D. Miller, W. Gentry, H. Pauly, D. Bassi, U. Hefter, K. Bergman, M. Zen, J. Reuss, C. Meijdenberg, D. Abuerbach, M. Kappes, S. Leutwyler, U. Valbusa, U. Buck, Y. Lee, P. Dagdigian, S. Stolte, R. Düren, and S. Iannotta, *Atomic and Molecular Beam Methods: Vol. 1* (Oxford University Press, New York, 1998).
- [23] K. Luria, W. Christen, and U. Even, Generation and propagation of intense supersonic beams, *J. Phys. Chem.* **115**, 7362 (2011).
- [24] W. R. Gentry and C. F. Giese, Ten microsecond pulsed molecular beam source and a fast ionization detector, *Rev. Sci. Instrum.* **49**, 595 (1978).
- [25] D. Bahat, O. Cheshnovsky, U. Even, N. Lavie, and Y. Magen, Generation and detection of intense cluster beams, *J. Phys. Chem.* **91**, 2460 (1987).
- [26] U. Even, The Even-Lavie valve as a source for high intensity supersonic beam, *EPJ Tech. Instrum.* **2**, 17 (2015).
- [27] N. A. Lavie and U. Even, Even-Lavie valve, <https://sites.google.com/site/evenlavievalve/home>, accessed 11 March 2024.
- [28] E. Narevicius and M. G. Raizen, Toward cold chemistry with magnetically decelerated supersonic beams, *Chem. Rev.* **112**, 4879 (2012).
- [29] P. Haslinger, N. Dörre, P. Geyer, J. Rodewald, S. Nimmrichter, and M. Arndt, A universal matter-wave interferometer with optical ionization gratings in the time domain, *Nat. Phys.* **9**, 144 (2013).
- [30] N. Dörre, J. Rodewald, P. Geyer, B. von Issendorff, P. Haslinger, and M. Arndt, Photofragmentation beam splitters for matter-wave interferometry, *Phys. Rev. Lett.* **113**, 233001 (2014).
- [31] S. N. Vogels, T. Karman, J. Klos, M. Besemer, J. Onvlee, A. van der Avoird, G. C. Groenenboom, and S. Y. T. van de Meerakker, Scattering resonances in bimolecular collisions between radicals and H₂ challenge the theoretical gold standard, *Nat. Chem.* **10**, 435 (2018).
- [32] W. Christen, Stationary flow conditions in pulsed supersonic beams, *J. Chem. Phys.* **139**, 154202 (2013).
- [33] D. Pentlehner, R. Riechers, B. Dick, A. Slenczka, U. Even, N. Lavie, R. Brown, and K. Luria, Rapidly pulsed helium droplet source, *Rev. Sci. Instrum.* **80**, 043302 (2009).
- [34] K. Luria, N. Lavie, and U. Even, Dielectric barrier discharge source for supersonic beams, *Rev. Sci. Instrum.* **80**, 104102 (2009).
- [35] A. S. Palau, S. D. Eder, T. Andersen, A. K. Ravn, G. Bracco, and B. Holst, Center-line intensity of a supersonic helium beam, *Phys. Rev. A* **98**, 063611 (2018).
- [36] A. S. Palau, S. D. Eder, G. Bracco, and B. Holst, Neutral helium atom microscopy, *Ultramicroscopy* **251**, 113753 (2023).
- [37] S. D. Eder, A. Salvador Palau, T. Kaltenbacher, G. Bracco, and B. Holst, Velocity distributions in microskimmer supersonic expansion helium beams: High precision measurements and modeling, *Rev. Sci. Instrum.* **89**, 113301 (2018).
- [38] T. Reisinger, G. Bracco, S. Rehbein, G. Schmahl, W. E. Ernst, and B. Holst, Direct images of the virtual source in a supersonic expansion, *J. Phys. Chem. A* **111**, 12620 (2007).
- [39] A. Apfoldter, Wiederaufbau und test einer He-streuapparat und erste streuexperimente an amorpher sowie kristalliner SiO₂-oberfläche, Master's thesis, Graz University of Technology, 2005.
- [40] S. D. Eder, A neutral matter-wave microscope (NEMI): Design and setup, Ph.D. thesis, University of Bergen, 2012.
- [41] H. Hotop, 11 - Detection of metastable atoms and molecules, in *Atomic, Molecular, and Optical Physics: Atoms and Molecules* edited by F. Dunning and R. G. Hulet, Experimental Methods in the Physical Sciences Vol. 29B (Academic Press, New York, 1996), pp. 191–215.
- [42] L. Pedemonte and G. Bracco, Study of He flow properties to test He dimer potentials, *J. Chem. Phys.* **119**, 1433 (2003).
- [43] J. P. Toennies and K. Winkelmann, Theoretical studies of highly expanded free jets: Influence of quantum effects and a realistic intermolecular potential, *J. Chem. Phys.* **66**, 3965 (1977).
- [44] W. Christen, K. Rademann, and U. Even, Supersonic beams at high particle densities: Model description beyond the ideal gas approximation, *J. Phys. Chem. A* **114**, 11189 (2010).
- [45] W. Christen and K. Rademann, Quantitative study of ⁴He real gas effects using supersonic beams, *Z. Phys. Chem.* **225**, 517 (2011).
- [46] R. D. McCarty and V. D. Arp, A new wide range equation of state for helium, in *Advances in Cryogenic Engineering: Parts A & B*, edited by R. W. Fast (Springer, Boston, 1990), Vol. 35, pp. 1465–1475.
- [47] U. Even, Pulsed supersonic beams from high pressure source: Simulation results and experimental measurements, *Adv. Chem.* **2014**, 636042 (2014).
- [48] U. Even (private communication).